THE PENNSYLVANIA STATE UNIVERSITY
SCHREYER HONORS COLLEGE

DEPARTMENT OF AEROSPACE ENGINEERING

DESIGN OPTIMIZATIONS FOR TURBULENCE REDUCTION OF A CLOSED-CIRCUIT AND COMPRESSED AIR WIND TUNNEL

JASON FINK
SPRING 2021

A thesis
submitted in partial fulfillment
of the requirements
for a baccalaureate degree
in Aerospace Engineering
with honors in Aerospace Engineering

Reviewed and approved* by the following:

Mark A. Miller
Assistant Professor of Aerospace Engineering
Thesis Supervisor

Philip J. Morris
Professor of Aerospace Engineering
Honors Adviser

* Electronic approvals are on file.

ABSTRACT

Previous work on closed-circuit wind tunnel design have shown that using mesh screens can prevent turbulence and flow separation by inhibiting excessive boundary layer growth. There are advantages and disadvantages to using a closed return wind tunnel. It is advantageous to use one because the flow can be better controlled as this will be discussed further in the design considerations. The main disadvantage is that closed return tunnels are larger and require more materials to make fully functional. Therefore, the cost for these types of wind tunnels are higher than an open return wind tunnel. The goal for the new facility at Penn State is to achieve high pressures (500psi), and in result, high Reynold's numbers using a pressure vessel. In this work, design optimizations were developed for the wide-angle diffuser, flow conditioning region, nozzle, test section, and the return diffuser to make the flow move more efficiently by mitigating unsteady flow and minimizing flow separation and turbulence. Several unique regions of the tunnel is its wide-angle diffuser, nozzle, and test section. The wide-angle diffuser is a short diffuser with a large area ratio and cone angle that requires its boundary layer growth to be controlled to prevent flow separation. The motivation for the wide-angle diffuser was to receive a large area ratio while keeping the length of the diffuser shorter than a typical diffuser would to save space within the facility. A typical diffuser would achieve the same area ratio with a longer length. It was decided to use one screen with a pressure loss coefficient of 2.65. The uniqueness of the nozzle was to include a point of inflection in its wall shape. Two cubic equations, one that describes the wall shape before the chosen inflection point, and one that describes the wall shape after the chosen inflection point, make up the contraction contour. Finally, the large diameter of the test section is important for the purpose of allowing large models to be tested such as aircraft

models, airfoils, and wind turbines. Recommendations for future work will be made depending on the data received when eventually testing all of these design considerations.

TABLE OF CONTENTS

LIST OF FIGURES iv

LIST OF TABLES v

ACKNOWLEDGEMENTS vi

Chapter 1 Information 1

- Pressure drop loss coefficients 3
- Wide-Angle Diffuser 3
- Flow conditioning and the settling chamber 6
- Nozzle and flow contraction 7
- The test section and the return diffuser 8
- Design considerations and using screens and honeycombs 8

Chapter 2 Design Considerations 13

- Wide-Angle Diffuser 13
- Flow conditioning and the settling chamber 14
- Nozzle contraction 15
- Corners or Elbows 17

Chapter 3 Design Process in CAD 19

- SolidWorks and OnShape 19

Chapter 4 Results (K Calculations) 22

- Wide-Angle Diffuser 22
- Flow conditioning and the settling chamber 23
- Nozzle contraction 25

Chapter 5 Discussion and Analysis of Results 28

- Future Work and Scale model 29

Chapter 6 Conclusion 31

REFERENCES 33

LIST OF FIGURES

Figure 1: General design of wind tunnel with labeled parts. 2

Figure 2: Area ratio with respect to total pressure loss coefficient for diffusers with screens. 5

Figure 3: Total diffuser angle and total screen loss with respect to area ratio. 6

Figure 4: Total diffuser angle with respect area ratio. 6

Figure 5: Quick change in wall shape prone to separation as flow comes from corner to diffuser inlet. 14

Figure 6: Nozzle wall shape design with inflection point at x = 50 in. 16

Figure 7: Contour before inflection and contour after inflection superimposed. 17

Figure 8: Wind tunnel elbows being manufactured. 18

Figure 9: Wide-angle diffuser. 20

Figure 10: Flow conditioning and settling chamber. 20

Figure 11: Nozzle. 21

Figure 12: Assembly of the pressure vessel. 21

Figure 13: Total closed-circuit wind tunnel original design from manufacturer.....21

Figure 14: Potential design for weld bands in pressure vessel. 30

LIST OF TABLES

Table 1: Flow conditioning screen information and calculations. 25

Table 2: Variables used to calculate section loss coefficients…….. 27

Table 3: Summary of section loss coefficients……..... 27

ACKNOWLEDGEMENTS

The author would like to thank Professor Mark A. Miller for his time and guidance for this undergraduate thesis. His extensive knowledge and experience in experimental aerodynamics and fluid mechanics allows him to be able to explain difficult concepts in an easy way for students to understand, resonate with and become inspired. The author would also like to thank his family and friends who are always very supportive and always provide valuable insight.

Chapter 1

Information

Wind tunnels are common tools that engineers use to run fluid mechanics experiments on models for data collection and research. Closed-circuit wind tunnels are particularly advantageous because they are designed to provide a controlled flow return. The downside to these types of wind tunnels are that they can be costly and take up more space. It is a challenge for traditional wind tunnels to match full-scale aerodynamics by duplicating the Reynold's number on small models. Because of this, compressed air was used as the working fluid to achieve a larger density, and thus a larger Reynold's number. The general structure of the Pennsylvania State University closed-circuit wind tunnel consists of a powered fan to move the fluid around the circuit, a twenty-five degree wide-angle diffuser for flow expansion with an area ratio of four, a flow conditioning section to suppress turbulence, a nozzle or flow contraction region to accelerate the flow, a test section for data collecting, and a return diffuser to ease the flow back to the fan. The wide-angle diffuser, flow conditioning section, and nozzle make up the wind tunnel's pressure vessel. The parts of the tunnel are shown in **Figure 1** below. The tunnel was designed for the working fluid to be compressed in a pressure range of more than 500 psi, thus providing a large Reynolds number without needing a relatively large velocity. This is accomplished using the ideal gas law because the relationship

$$R_e = \frac{\rho VL}{\mu} = \frac{PVL}{\mu RT} \text{ since } P = \rho RT \tag{1}$$

shows that density, and therefore, pressure is directly proportional to the Reynold's number. In these equations, ρ is the density of the fluid, V is its velocity, μ is its dynamic viscosity, L is the characteristic linear dimension, P is the pressure, R is the gas constant, and T is the temperature. The freestream velocity for this tunnel is approximately 82 ft/s. Experiments that are planned to be completed using this tunnel will be done on rotor-craft, wind turbines, propellers, and fans to learn more about the rotational augmentation effect. Rotational augmentation is an effect studied on rotating airfoils such as helicopters and wind turbines [9].

The design considerations that were taken into account were to attempt to minimize the probability of flow separation and reduce any turbulence, both axial and lateral turbulence. The current work was aimed at optimizing the wind tunnel design, and focused on several critical sections including the pressure vessel, test section, and return diffuser. Each of these sections, broken into five different regions, will be covered in this report.

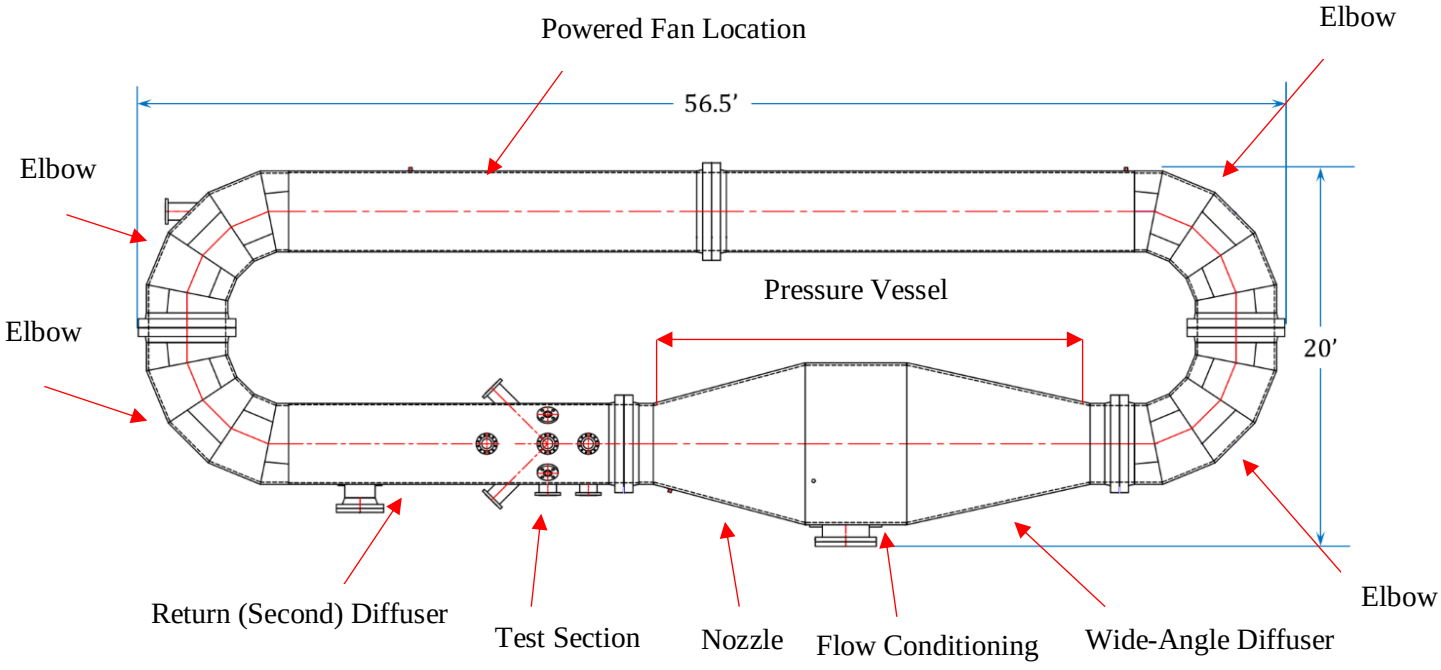

Figure 1: General design of wind tunnel with labeled parts.

Pressure drop loss coefficients

Pressure drop losses often occur within closed-circuit wind tunnels in regions where the flow is most likely to separate and deviate from smooth, steady flow. The pressure drop coefficient is defined by the ratio of the static pressure drop, Δp, divided by the dynamic pressure, q [2]. Therefore,

$$K = \frac{\Delta p}{q}, \text{ where } q = \frac{1}{2}\rho v^2 \text{ [2].} \quad (2)$$

Because the pressure loss is related to the dynamic pressure, it is common to reference loss coefficients to the test section dynamic pressure. The pressure drop coefficient may be calculated across mesh screens and in various regions throughout the wind tunnel. They may also be calculated for each section of the wind tunnel to see which regions contribute the most losses and are most likely to experience flow separation.

Wide-Angle Diffuser

A diffuser is used in a wind tunnel to slow down and expand the flow. The wide-angle diffuser is typically used in a wind tunnel when the laboratory has space constrictions, but a large diffuser area ratio and a large contraction ratio are desired [1-2]. Because of space constrictions, one of the wide-angle diffuser's purposes is to decrease the length of the diffuser of a given area ratio, which was four in our case [2]. Due to the nature of the angle and length, the wide-angle diffuser is large and is another region of potential flow separation. Typically, in diffusers, the probability of flow separation increases as the flow continues further downstream. A flat piece of

sheet metal will be appended to the inlet of the wide-angle diffuser to ease the flow into expansion. This is necessary because the diffuser inlet is very close to the end of the corner prior to the diffuser. It is located between the second corner counting from the fan and the flow conditioning settling chamber region of the wind tunnel. The difficulty of using a wide-angle diffuser is that the cross-sectional area increases quickly, increasing the probability of flow separation which may only be solved by boundary layer control [2]. It is recommended to use many screens in a wide-angle diffuser with a relatively low value for the pressure drop coefficient, K, that sums up to the desired K [2]. However, we used a single screen as this may be all that is necessary to prevent flow separation. One screen was chosen out of convenience and as a place to start to see how the flow will react to it and to see if it will be successful in preventing flow separation. The screen will be placed approximately two thirds of the way downstream the diffuser. This is because as the flow travels further downstream a diffuser, the increasing cross-sectional area ratio increases the probability of flow separation. Therefore, this region was most likely where the flow would separate. **Figure 2** from Mehta represents the total K with respect to the area ratio A_R for diffusers with screens and is used for design considerations. Because our $A_R = 4$, we could design the diffuser such that the total K for the screens in the diffuser is approximately 2.65 [2]. Also, because of the location on the plot, it is recommended that curved screens be used [2]. This is denoted by the circular points on the chart. **Figure 3** from Jewel Barlow, William Rae, and Alan Pope shows in the first subplot that successful operation for the diffuser could be completed using between zero and one screen [1]. The second subplot shows a similar approach to designing the proper pressure loss coefficient by showing that at an area ratio, $A_R = 4$, the diffuser angle, $2\theta = 25$ degrees and the total screen loss is approximately 2.65 [1]. **Figure 4** from Mehta proved that only one screen was necessary as the

diffuser angle for the wide-angle diffuser was 25 degrees and the area ratio was 4 [2]. The circles on the chart represent diffusers with circular cross section shapes and the rectangles on the chart represent diffusers with rectangular cross sections. Their locations state which diffuser was tested with angle and area ratio. The horizontal lines above the cross-sectional shape represent the number of screens that were unsuccessful and the horizontal lines below the cross-sectional shape represent the number of screens that were successful. The 'X' inside the diffuser shape shows which diffusers had straight walls and the dots show the diffusers with curved walls. This study did not test a diffuser with the same parameters as the one in this thesis, but it still provided useful information regarding wide angle diffusers. Because of these findings, one screen with a designed K of 2.65 will be tested in our first pass.

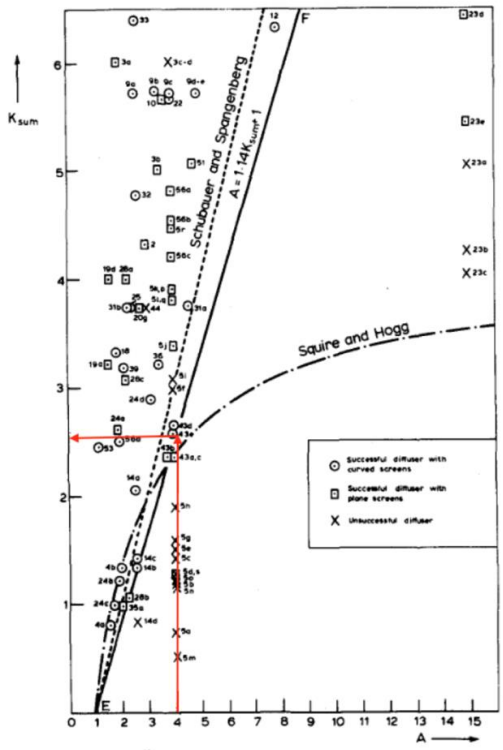

Figure 2: Area ratio with respect to total pressure loss coefficient for diffusers with screens.

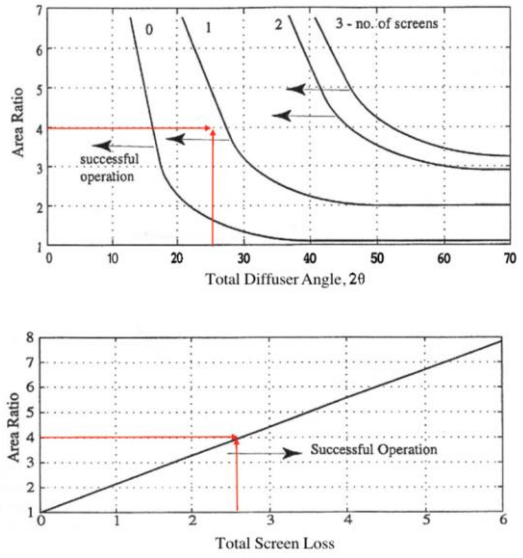

Figure 3: Total diffuser angle and total screen loss with respect to area ratio.

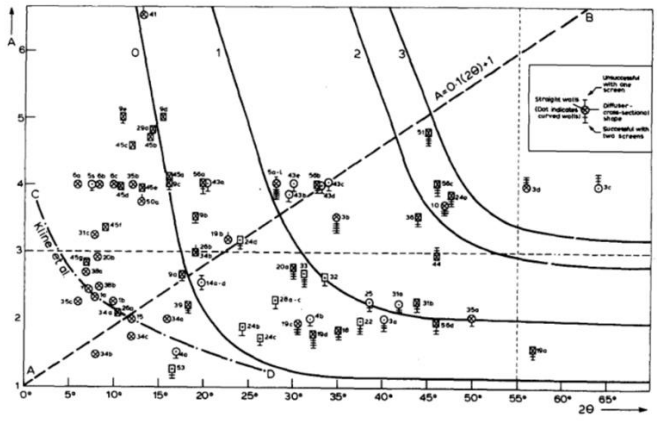

Figure 4: Total diffuser angle with respect area ratio.

Flow conditioning and the settling chamber

A flow conditioning region is a location where the turbulence caused by mean velocity variations in the flow are to be minimized. The flow conditioning section design considerations were mainly concerned with minimizing axial and tangential turbulence. In order to achieve this,

three screens and honeycombs will be used. The honeycombs will reduce all non-axial turbulence designated by the velocities v' in the y-direction and w' in the z-direction. The three screens will have different wire diameters and therefore, different screen solidities. Their purpose will be to control turbulence and help straighten out the flow. They will do this by reducing the u' turbulence in the x-direction. Because the wind tunnel has a circular test section, the rest of the tunnel including the flow conditioning and settling chamber has a circular cross section. The settling chamber region of the flow conditioning section is located toward the exit of the region. That is, beyond the last screen and just before contraction.

Nozzle and flow contraction

The Nozzle contracts and accelerates the flow at high speeds into the test section. Accelerating the flow will reduce the mean-flow nonuniformities to produce an even velocity profile at the inlet of the test section, the relative turbulence level will be reduced, and the dynamic loads and screen and honeycomb losses will be reduced because of the reduced dynamic pressure in the settling chamber [5]. Nozzles may be designed to have inflection points where the wall shape can be customized to change how the flow is accelerated into the test section. The inflection point is the region along the wall shape where the curve changes allowing the exit diameter to be smaller than the inlet diameter. To create a wall shape with a smooth contour for which an inflection point exists, we used cubic equations. Third order polynomial equations were used even though fifth order polynomial equations provide uniform flow and no flow separation [8]. The risks of using a third order polynomial wall shape were highlighted in Bell and Mehta's contraction design paper. It was stated that flow was attached, but was not

uniform [8]. Because keeping the flow attached in contraction is a priority, a third order polynomial wall shape is suitable.

The test section and the return diffuser

Once the flow is accelerated by the nozzle and it leaves the exit diameter, it enters directly into the test section. The test section has a circular cross section with a maximum diameter of 40in and a minimum diameter of 20in. This is a relatively large test section that will allow Penn State to run many different kinds of tests. Currently, the main test models that are being considered are wind turbine and helicopter rotors, airfoils, full aircraft models, propellers, fans, and UAV models. The test section will also consider complex and unsteady three-dimensional flow systems and do phase-lock imaging of the flow on or near the rotor blade for wake imaging. The test section will contain windows, static pressure ports, and a breather slot. Toward the end of the test section will be a return diffuser. The function of this second diffuser is to re-expand and slow the flow bringing it back to the wind tunnel tubing diameter. The return diffuser will send the flow around back to the fan and to the first elbow.

Design considerations and using screens and honeycombs

Screens are most efficient when placed such that the flow enters orthogonally to the mesh. That is, the streamlines of the flow enter the screens at right angles [2]. Therefore, many tunnels use screens that curve across the diameter of the section as opposed to be placed straight across the diameter [2]. It is necessary to used curved screens when the wall is sloped such as the

wall inside the diffuser. The function of the screens is to reduce the probability of flow separation in locations separation is likely. Potential locations are where the diffuser wall angle changes, where the elbows turn, non-smooth entry or exit from the pressure vessel, or anywhere with excessive boundary layer growth. Therefore, the screens act to control the boundary layer. They make the flow velocity profiles more uniform by causing a static pressure drop proportional to the speed leading to a decrease in boundary layer thickness so that it can better withstand larger pressure gradients and prevent flow separation [4]. By refracting the incident flow toward the local normal, the turbulence intensity of the flow field is reduced [4]. Other integral properties of the screens are to reduce the mean velocity variation to prevent flow separation, reduce turbulent fluctuations, and refract inclined flow toward the local normal to the screen [2]. Using multiple screens with a low K for a given pressure loss leads to a greater reduction in turbulence intensity [2]. The equation for finding the pressure loss across a screen may be defined in lieu of the screen solidity by Collar's method,

$$K_C = \frac{C(1-\beta)}{\beta^2} \tag{3}$$

where C is a constant and assumed to be 1 [2]. However, this approach was replaced by Tavoularis's method that relates K to the Reynold's number with the characteristic linear dimension being the wire diameter and the screen solidity only [3]. Another design feature used in the tunnel is honeycombs. Honeycombs may be used to remove swirl and lateral mean velocity variations and turbulence [2]. Honeycomb shapes usually have a hexagonal cross-section [2]. In order to make honeycombs effective at suppressing turbulence, it is typical to use

small cell sizes and have 150 cells per settling chamber diameter which is the ratio of the number of cells to the diameter [2].

Nomenclature

P	Pressure
R	Ideal gas constant of the working fluid
T	Temperature
ρ	Density of the working fluid
Δp	Static pressure drop
K	Pressure loss coefficient (subscripts 1, 2, 3 relate to flow conditioning screens 1, 2, 3)
q	Dynamic pressure
A_R	Area ratio of wide-angle diffuser
2θ	Total wide-angle diffuser angle
u’	Mean velocity variation in the x-direction
v’	Mean velocity variation in the y-direction
w’	Mean velocity variation in the z-direction
V	Freestream velocity in wind tunnel
Δp_f	Static pressure drop due to pipe friction law
V_n	Local section mean speed
f	Friction factor
R_e	Reynold’s number (subscripts 1, 2, 3 correspond to flow conditioning screens 1, 2, 3)
K_{nl}	Nozzle pressure loss coefficient due to friction using Wattendorf’s formulation
d_w	Wire diameter
D	Section diameter (subscripts correspond to specific section)

w_m	Opening size
ρ_m	Screen mesh density
μ	Dynamic viscosity
β_s	Screen porosity
σ_s	Screen solidity
K_C	Loss coefficient of wide-angle diffuser using Collar's method
K_d	Total loss coefficient of wide-angle diffuser (sum of K_f and K_{ex})
W_i	Nozzle inlet width
W_e	Nozzle exit width
x_m	Inflection point in nozzle
L	Projected length (used for nozzle wall shape equation) or characteristic linear dimension (used for Reynold's number)
K_{sum}	Total screen loss coefficient
K_f	Pressure loss due to friction in wide-angle diffuser
K_{ex}	Pressure loss due to flow expansion in wide-angle diffuser
$K_e(\theta)$	Wide-angle diffuser loss coefficient of circular cross section and $5° < \theta$
K_{nt}	Nozzle loss coefficient using Wattendorf's approximation
K_t	Total losses in wind tunnel pressure vessel

Chapter 2

Design Considerations

Wide-Angle Diffuser

The wide-angle diffuser has a length of 126in and a linearly increasing cross-sectional area downstream such that the inlet diameter is 4ft and the exit diameter is 8ft. However, the diameters are better represented as the area ratio. A point of concern with this location is the quick change in wall shape from the wind tunnel tubing to the inlet of the diffuser as shown in **Figure 5**. Because this transition is not smooth, the sheet metal should smooth out the flow and prevent pressure losses and flow separation due to boundary layer growth here. As stated previously, a single mesh screen will be placed two thirds of the way down the diffuser or approximately 84in along the diffuser's length. This is a good location for a screen because it is not at the diffuser's exit, but it is still located far downstream. Because the literature recommended using several screens of low K that add up to the total pressure loss as opposed to a single screen with the value of the total pressure loss, two screens will likely be tested, but may not be required. This is not a current concern as **Figure 4** represented that for this specific diffuser angle, zero to one screen should be efficient.

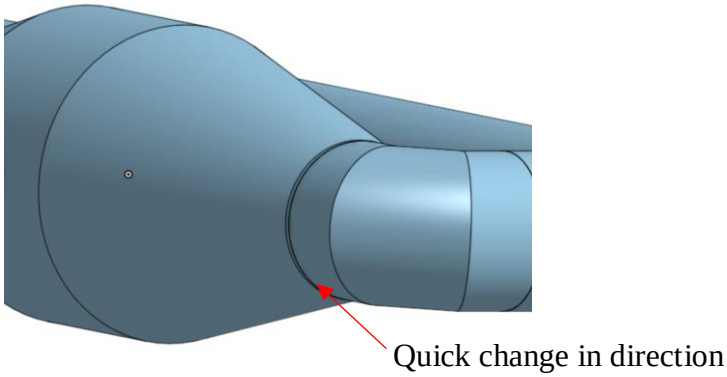

Figure 5: Quick change in wall shape prone to separation as flow comes from corner to diffuser inlet.

Flow conditioning and the settling chamber

The cylindrical flow conditioning section has an inlet and exit diameter of 8ft and a length of 60in. The flow conditioning and settling chamber design considerations were made to reduce turbulence by attempting to remove mean velocity variations in the flow. Hexagonal-shaped honeycombs will be implemented directly at the inlet of this region. Because this location is downstream the wide-angle diffuser exit, the flow static pressures and angles have the opportunity to become more uniform [4]. As stated previously, the honeycombs function to suppress the v' and w' velocity variations and the off-axis turbulence. However, they will not be effective in reducing the axial turbulence caused by u'. For this, three screens will be spaced out evenly further downstream the flow conditioning region. For the first pass, the screens will be placed approximately 0.2 settling chamber diameters from each other with 0.2 settling chamber lengths between the last screen and the flow conditioning exit [4]. This setup allows for the static pressure to fully recover, $\frac{dp}{dy} = 0$ before reaching the next screen [4]. Because the diameter of the settling chamber is 8ft, the screens will be placed 1.6ft apart from each other with the third

screen placed 1.6ft before the settling chamber exit. Also, the screens' wire diameters will be decreasing in size as the flow travels downstream the settling chamber. As stated previously, the first screen will have a wire diameter of 0.009in, the second screen will have a wire diameter of 0.0085in, and the third screen will have a wire diameter of 0.0065in. The third screen will have the smallest screen solidity and smallest loss coefficient and the second screen will have the largest screen solidity and largest loss coefficient.

Nozzle contraction

The function of the nozzle is to simply accelerate the flow into the test section. The nozzle's original design had a linear wall shape that brings the flow from the settling chamber's exit diameter of 8ft to the test section's inlet diameter of 40in. Also, it had a defined length of 107in. A more ideal nozzle wall shape follows a cubic polynomial and contains an inflection point where the wall shape's curve changes direction. Creating a wall shape that has an inflection point allows for the remainder of the section to be customized such that the flow can be controlled in various ways. By changing the value of x_m, the wall shape can be changed. The value for x_m that was used was 50in to provide a nicely shaped curve for the flow to accelerate. The new design for the nozzle has a length of 100in because maintaining the 107in length does not allow for the nozzle exit to have a zero slope. It is important for the inlet and exit of the nozzle to have a zero slope because an excess wall curvature causes adverse pressure gradients near the inlet and exit [6]. Adverse pressure gradients cause the boundary layer to thicken and increase the probability of flow separation [6]. In order to design the third order wall shape, the equation,

$$\frac{y}{\frac{W_e}{2}} = \frac{W_i}{W_e} + (1 - \frac{W_i}{W_e}) \frac{(\frac{x}{L})^3}{(\frac{x_m}{L})^2} \quad (4)$$

was used to describe the wall shape prior to the inflection point [5]. That is, when $0 < x < x_m$ where x is the local length of the nozzle and x_m is the x-coordinate of the chosen inflection point [5]. The wall shape after the point of inflection was described using the equation,

$$\frac{y}{\frac{W_e}{2}} = 1 + (\frac{W_i}{W_e} - 1) \frac{(1-\frac{x}{L})^3}{(1-\frac{x_m}{L})^2} \quad (5)$$

when $x_m < x < L$ [5]. W_i and W_e are the widths of the cross section of the inlet and exit respectively, L is the projected length of the nozzle, and x_m is the inflection point.

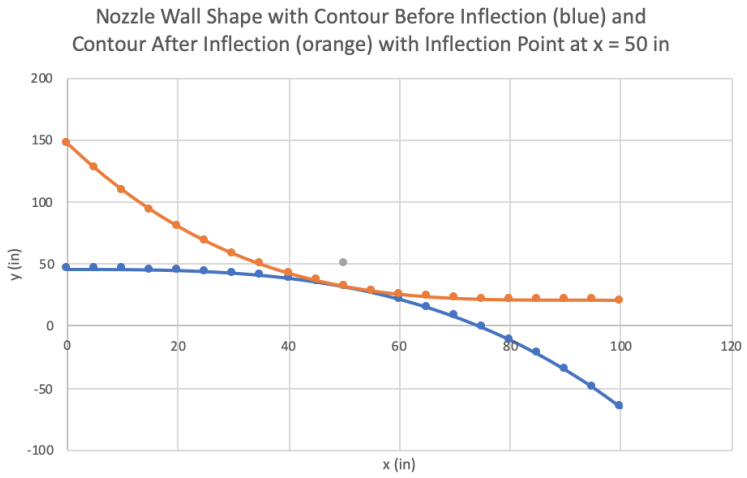

Figure 6: Nozzle wall shape design with inflection point at x = 50 in.

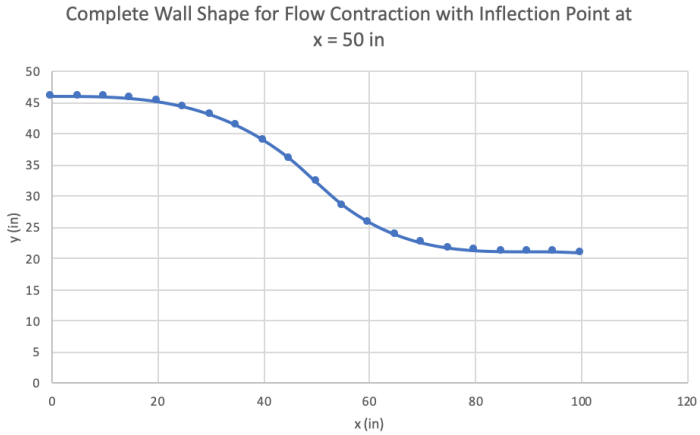

Figure 7: Contour before inflection and contour after inflection superimposed.

Figure 6 and **Figure 7** were used to calculate and plot the true wall shape and test various inflection points to see which inflection was optimal. It was decided that the wall shape with the inflection point at x = 50, approximately halfway downstream the nozzle inlet, was most the suitable design.

Corners or Elbows

Although the corners of the wind tunnel were beyond the scope of the thesis, understanding how the flow moves around the elbows provided insight for the design considerations for the pressure vessel, test section, and return diffuser. The four corners of the closed-circuit wind tunnel are relatively sharp and move the flow around themselves fairly quickly. Because of this, they are a potential region where the flow will see pressure drops. Therefore, the flow needs to be taken around each corner more gradually. To do this, turning vanes will be implemented to help the flow move around each corner. The turning vanes may

also reduce the pressure gradient on the wall of the corner [2]. **Figure 8** shows the elbows currently being manufactured.

Figure 8: Wind tunnel elbows being manufactured.

Chapter 3

Design Process in CAD

SolidWorks and OnShape

The original design for the wind tunnel was created in the computer aided design (CAD) software called OnShape. This model was from the manufacturer and was used to come up with the design optimizations discussed throughout this paper. The design for the wide-angle diffuser, the flow conditioning and settling chamber, and the nozzle were also remodeled in CAD using SolidWorks. The wide-angle diffuser is shown in **Figure 9** and has a length of 126in, an inlet diameter of 46in, and an exit diameter of 91.8in. It also has a bolting flange where the bolt diameters are 0.4531in. The outside diameter of the flange is 96.836in. The flow conditioning section in **Figure 10** has a diameter of 91.8in and an outside flange diameter of 96.8in. The bolt diameters are also 0.4531in as this piece will be directly connected to the outlet of the wide-angle diffuser. **Figure 11** shows the nozzle with a length of 100in and an inflection point at 50in. This region has an inlet diameter of 91.8in and will be attached directly to the outlet of the flow conditioning section. It has an outside flange diameter of 97.2in and a bolt diameter of 0.4531in. The exit diameter of the nozzle is 41.76in as this piece will be directly attached to the inlet of the test section. Finally, the pressure vessel was assembled in **Figure 12**. This assembly contains the wide-angle diffuser, the flow conditioning section, and the nozzle. This figure gives the opportunity to see how all the pieces fit together by bolting. **Figure 13** shows the manufacturer's original CAD model of the entire wind tunnel using OnShape. This model is a preliminary model and not a final design because its elbows are incorrect. It was used to make the necessary design changes and see how the flow will travel throughout the tunnel.

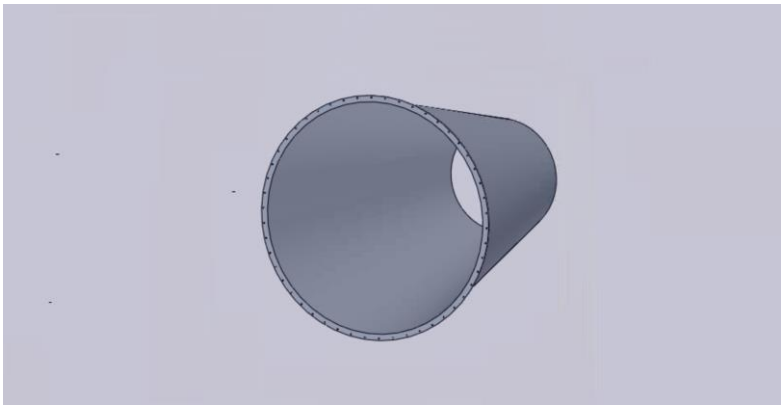

Figure 9: Wide-angle diffuser.

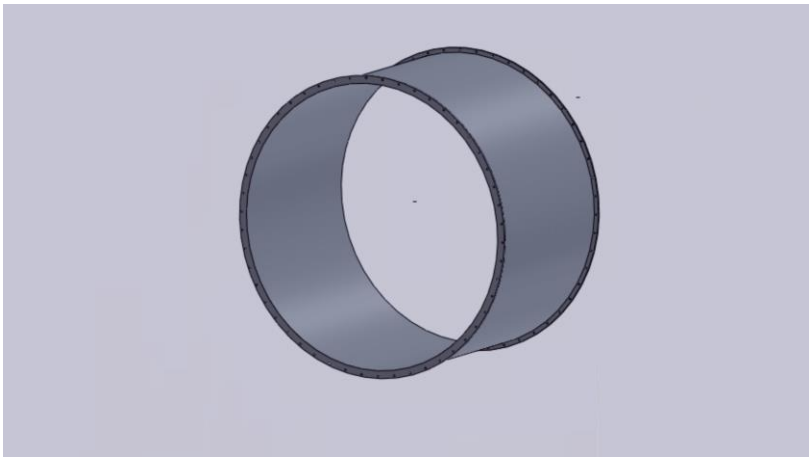

Figure 10: Flow conditioning and settling chamber.

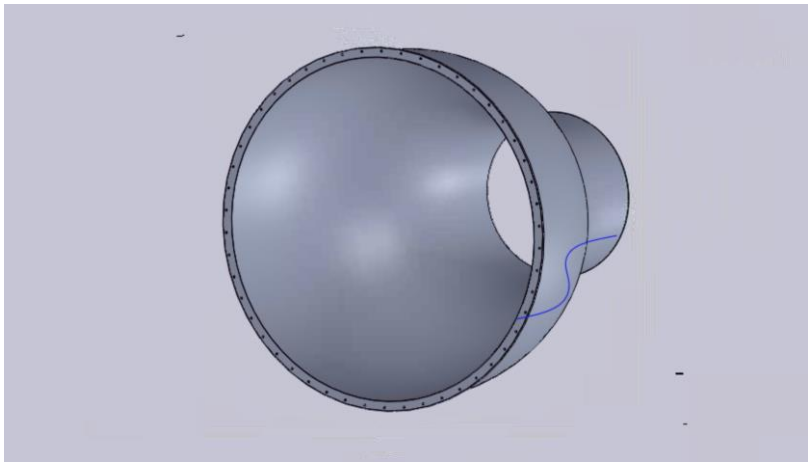

Figure 11: Nozzle.

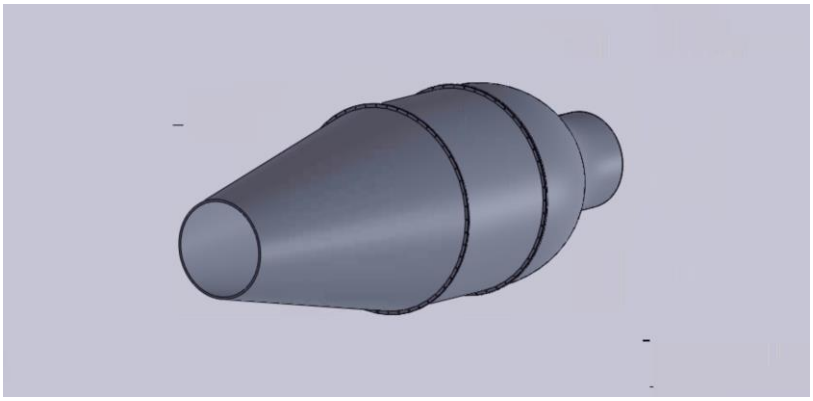

Figure 12: Assembly of the pressure vessel.

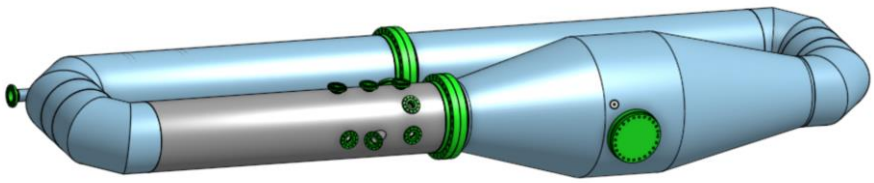

Figure 13: Total closed-circuit wind tunnel original design from manufacturer.

Chapter 4

Results (K Calculations)

Wide-Angle Diffuser

To calculate the loss coefficient of the wide-angle diffuser, the losses due to flow expansion, K_{ex}, and the losses due to friction, K_f, were summed [1]. The losses due to friction were calculated using

$$K_f = \left(1 - \frac{1}{A_R^2}\right) * \frac{f}{8\sin(\theta)}, \tag{6}$$

and the losses due to flow expansion were calculated using

$$K_{ex} = K_e(\theta)\left(\frac{A_R - 1}{A_R}\right)^2 \tag{7}$$

where

$$K_e(\theta) = -0.09661 + 0.046728\theta \tag{8}$$

for a circular cross section where $5° < \theta$ [1]. The friction factor, f, is a friction coefficient that is found using the iterative solution,

$$f = 2log_{10}\left(R_e\sqrt{f}\right) - 0.8 \tag{9}$$

The value for f becomes accurate with at least four iterations because the value converges [1]. **Table 2** shows a summary of the variables used to calculate the K values for the wide-angle diffuser. The screen used to calculate the screen loss coefficient in the wide-angle diffuser had the same wire diameter, opening size, and mesh density as the first screen in the flow conditioning section. The screen porosity was calculated using equation (10) and the screen's solidity was calculated using equation (11). The values for the porosity and solidity were consistent with that of the first screen in the flow conditioning section. The value for the diffusers K is shown in **Table 3**. Because K of the diffuser is the sum of the K due to friction and the K due to flow expansion, the K of the diffuser was calculated to be 1.2742. This value is different from the value derived from the charts in the introduction that showed the K should be around 2.65. Since the calculated value did not match the expected value, further revisions of the calculation will be made in future work.

Flow conditioning and the settling chamber

The three screens of choice have a wire diameter of 0.009in, 0.0085in, and 0.0065in respectively. It was decided to have the wire diameters decrease in size as the flow travels through because it allowed us to choose the opening sizes to decrease with wire diameter with the exception of screen three. The opening size is the open space measured between the centers of two wires. In order to find the screen loss coefficient for each screen, the screen porosity, β_s, and the screen solidity, σ, were calculated. Desired screen solidities are in the range of 0.50-0.80 [1]. The screen porosity is a function of wire diameter and weave or mesh density, ρ_m, which is

simply $\frac{1}{w_m}$ where w_m is the opening size [1]. The screen porosity was calculated using the equation,

$$\beta_s = (1 - \frac{d_w}{w_m})^2 \text{ [1].} \tag{10}$$

The values for the screen porosities are summarized in **Table 1** below. With the screen porosity, it was easy to calculate the screen porosity using the relationship,

$$\sigma = 1 - \beta_s \text{ [1].} \tag{11}$$

The screen solidities are also summarized in **Table 1** below. The values fell within the desired range that was proposed by Barlow, Rae, and Pope. The Reynold's number for each screen was calculated using the equation

$$Re_{d_w} = \frac{\rho V d_w}{\mu} \tag{12}$$

where ρ is the density of the working fluid, V is the velocity, μ is the dynamic viscosity, and d_w is the wire diameter. The Reynold's numbers for the screens 1, 2, and 3 were denoted R_{e1}, R_{e2}, and R_{e3} respectively in **Table 2**. Finally, using equation

$$K = (0.52 + \frac{17}{Re_{d_w}}) \frac{\sigma(2-\sigma)}{(1-\sigma)^2}, \tag{13}$$

the screen loss coefficients were able to be calculated [3]. This equation for screen loss coefficients shows that $K \in \{Re_{d_w}, \sigma\}$ where Re_{d_w} is the Reynold's number of the flow through the screen. The values for the screen loss coefficients are also summarized in **Table 1** below along with the total losses due to the flow conditioning screens by taking the sum of the three values.

Screen	*Wire Diameter d_w (in)*	*Opening Size w_m (in)*	*Mesh Density ρ_m (in^{-1})*	*Screen Porosity β_s*	*Solidity*	*Loss Coefficient K*
1	0.009	0.022	45.455	0.3492	0.6508	0.7959
2	0.0085	0.017	58.824	0.25	0.75	1.119
3	0.0065	0.0185	54.054	0.4207	0.5793	0.6473
Total						2.562

Table 1: Flow conditioning screen information and calculations.

The final K values for screens 1, 2, and 3 were found to be 0.7959, 1.119, and 0.6473 respectively and are shown in **Table 3**.

Nozzle contraction

The pressure loss coefficient was considered to be caused by friction only and is derived from the standard pipe friction law,

$$\Delta p_f = \int_0^{L_n} f \frac{\rho}{2} \frac{V_n^2}{D_n} dx \tag{14}$$

where L_n is the length of the nozzle, D_n is the nozzle hydraulic diameter, V_n is the local section mean speed defined as,

$$V_n^2 = V_{SC}^2 (\frac{D_{SC}}{D_n})^4 \quad (15)$$

with the subscript SC defined for the settling chamber, and f is a friction coefficient that is found using the iterative solution,

$$f = 2log_{10}(R_e\sqrt{f}) - 0.8 \quad (16)$$

where R_e is the Reynold's number [1]. Therefore, the pressure loss coefficient due to friction in the nozzle is approximated by

$$K_{nl} = f_{av} \frac{L_n}{D_{ts}} \int_0^1 \frac{D_{ts}^5}{D_n^5} d(\frac{x}{L_n}), \quad (17)$$

with the subscript, ts, referring to the test section and the subscript, av, referring to the average iterative value of f [1]. This equation may be further approximated by Wattendorf's formulation

$$K_{nl} = 0.32 f_{av} \frac{L_n}{D_{ts}} \text{ [1].} \quad (18)$$

The value for the pressure loss coefficient of the nozzle was found to be 0.001285 and is shown in **Table 3**. This value seemed too low and will need calculation revisions in future work. Finally, **Table 3** summarizes all loss coefficients calculated. This table includes the screen loss coefficients for the three screens in the flow conditioning region from **Table 1** for completeness. It also includes a variable, K_t, representing the total sum of all loss coefficients within the

pressure vessel. The total pressure loss coefficient for the entire pressure vessel is the sum of the K values for the wide-angle diffuser, the flow conditioning section, and the nozzle. This value was shown in **Table 3** and was calculated to be 5.112.

Variable	*Value*
A_R	4
θ	12.5°
f	0.004057
d_w	0.009in
w_m	0.022in
ρ_m	45.455in^{-1}
β_s	0.3492
σ	0.6508
ρ	33.799$\frac{kg}{m^3}$
μ	2.146x10^{-5}Pa*s
V	25$\frac{m}{s}$
R_{e1}, R_{e2}, R_{e3}	9000, 8500, 6500
f_{av}	0.004196
L_n	7.917ft
D_{ws}	8ft

Table 2: Variables used to calculate section loss coefficients.

Pressure Loss (K)	*Value*
K_f	1
K_{ex}	0.2742
K_d	1.274
K_{nl}	0.001285
K_1	0.7959
K_2	1.119
K_3	0.6473
K_t	5.112

Table 3: Summary of section loss coefficients.

Chapter 5

Discussion and Analysis of Results

The wide-angle diffuser's loss coefficient was made up of two parts, the losses due to the flow expanding and the losses due to friction [1]. When the flow is expanded, it is slowed and as the area ratio is increased, the efficiency of the diffuser decreases [7]. Because the area ratio is relatively large, this drop in efficiency may have contributed to the diffuser losses. Also, as the angle of expansion increases, the flow becomes asymmetrical and separation is more likely to occur [7]. A diffuser with a large expansion ratio should decrease efficiency because there tends to be more losses. However, the diffuser has a circular cross-sectional area which is more efficient than a square diffuser [7]. The losses due to friction were greater than the losses due to expansion. This suggests that the diffuser's wall roughness may have been too much for its angle.

The honeycombs and screens in flow conditioning contribute to pressure losses, however, they function to suppress turbulence. Again, the screen solidities fit within their desired 0.6-0.8 range. It can be seen by the relationship between screen porosity and screen solidity that as the porosity decreases, the screen solidity increases. However, as the solidity increases, the loss coefficient, K, tends toward zero and when the solidity approaches zero, K converges to a value related to only the Reynold's number. In flow contraction, the velocity increases and the pressure decreases according to Bernoulli's Principle. In order to conserve mass, the flow must move faster as the cross-sectional area decreases downstream the nozzle. The energy needed to cause

the velocity of the flow to increase comes from the pressure. The transfer of the motion of the fluid particles to fast moving flow causes the pressure to drop.

Future Work and Scale model

There are several important considerations for future work on this project. Further calculations need to be worked out prior to testing models in the wind tunnel. The test section, return diffuser, corners, and fan loss coefficients need to be calculated. Also, as stated previously, revisions of the calculations for the wide-angle diffuser and nozzle loss coefficients need to be made. The K value calculated for the wide-angle diffuser was lower than expected from the charts used to estimate the value based on area ratio, diffuser angle, and total pressure losses. The K value calculated for the nozzle seemed to be too small and needs further calculations to determine the true value. More CAD models need to be designed with other options for how the sections of the tunnel will be connected to each other. For now, there is a conventional bolting method as seen from the figures. Another approach to bolting could be bolting from the inside of the tunnel as this may make it easier to put the sections together when they are done being manufactured. Also, more works on weld bands for the interior of the pressure vessel need to be completed. The purpose of the weld bands are to hold the screen in their respective areas, but it would be ideal to have weld bands that allow for easy changes in screen location. For example, if the wide-angle diffuser screen needs its location adjusted, it would be ideal to not have to move the weld bands. A potential design for them are shown in **Figure 14**. The length of the weld bands allows for easy adjustment of the screen because the screen can be moved along the bracket.

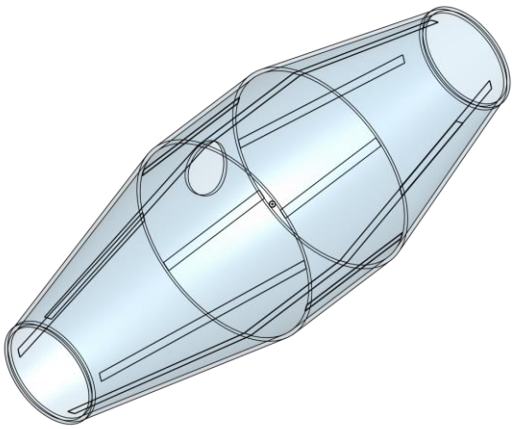

Figure 14: Potential design for weld bands in pressure vessel.

As part of the future works of this project, a 3-D printed scaled model of the wind tunnel between the pressure vessel and the return diffuser may be created. The purpose of the scale model is to try to replicate the flow through the sections of the tunnel and compute calculations regarding the flow prior to testing it in the real tunnel. The goal is to try getting similar data to the theoretical calculations on the actual wind tunnel. The working fluid for the scaled model will be water because it will help recreate the high Reynold's number of the compressed air being used in the actual tunnel. However, the Reynold's number will be inaccurate by nature. To make up for the inaccuracies, the velocity of the working fluid and the kinematic viscosity need to be balanced. The dry, compressed air will be traveling at a larger velocity and be placed under a larger pressure than the water in the scaled model. Important calculations under consideration are the loss coefficients in each section, the total pressure drop, the pumping power, the volume flow rate, the velocity in the test section, the static pressure in the flow conditioning section and test section, and the velocity in the contraction region using the change in pressure and the contraction ratio.

Chapter 6

Conclusion

The design considerations made for the wide-angle diffuser, the flow conditioning and settling chamber, the contraction nozzle, the test section, and the return diffuser will be implemented on the wind tunnel once it is done being manufactured. Once Penn State receives the wind tunnel, preliminary testing will be able to determine the accuracy of the theoretical calculations. However, it is important to include screens to prevent excessive boundary layer growth and flow separation. Also, it is important to include turbulence screens and honeycombs to reduce turbulent flow. It was also necessary to redesign the nozzle to provide it a cubic wall shape with an inflection point so that the flow can be altered for its entry into the test section depending on the model and tests being completed.

The decision for having one screen in the wide-angle diffuser was made as a first pass design consideration. Once the tunnel is completed, the screen will be tested to see if it effectively prevents flow separation. If it is necessary, an additional screen will be placed in a similar location downstream the diffuser. The reason this may be useful is because it is better to have multiple screens sum up to the loss coefficient value as opposed to having a single screen with the given loss coefficient. The nozzle inflection point was chosen due to its location being somewhere near the middle of the total length of the section. This is an ideal location for the point of inflection, but future simulations and testing using the scale model will help determine if this point needs to be slightly shifted.

The findings presented in this paper requires additional research. Additional testing will need to be completed once the wind tunnel is done being manufactured so that the design considerations presented in this paper may be finalized or improved. The design considerations

in the flow conditioning and settling chamber, test section and return diffuser will most likely be finalized, but testing needs to be completed to determine if the wide-angle diffuser needs additional screens and if the nozzle needs to have its inflection point shifted to a different location.

REFERENCES

[1] Barlow, Jewel B., et al. Low-Speed Wind Tunnel Testing. John Wiley & Sons, Inc.

[2] Department of Aeronautics, Imperial College, London, & Mehta, R. D. (1977). The Aerodynamic Design of Blower Tunnels with Wide-Angle Diffusers (Vol. 18 pp. 59-120). Pergamon Press Prog. Aerospace Sci.

[3] Tavoularis, S. (2009, August). Measurement in Fluid Mechanics. Cambridge University Press.

[4] Mehta, R. D., & Bradshaw, P. (1979, November). Design Rules for Small Low Speed Wind Tunnels. Aeronautical Journal.

[5] Brophy, C. M., & Reischman, M. Turbulence Management and Flow Qualification of the Pennsylvania State University Low-Speed, Low-Turbulence Closed Circuit Wind Tunnel.

[6] Arslanian, J., & Matin, P. (2012). Undergraduate Research on Conceptual Design of a Wind Tunnel for Instructional Purposes. American Society for Engineering Education.

[7] Lo, S. C. (1963). Frictional Losses in Conical Diffusers Having Wide Angles.

[8] National Aeronautics and Space Administration, Bell, J. H., & Mehta, R. D. (1988, August). Contraction Design for Small Low-Speed Wind Tunnels. NASA.

[9] Früh, Wolf-Gerrit. (2008). On the process of rotational augmentation. European Wind Energy Conference and Exhibition 2008. 6.

ACADEMIC VITA

Jason Fink
I am seeking to expand my knowledge in technology innovation, development, and advancement within medicine, financial markets and space exploration.

jasonfink09@gmail.com

Jfink09

EDUCATION

The Pennsylvania State University, University Park, State College, PA
Schreyer Honors College Scholar
Academic Scholarship Recipient
Major: *Aerospace Engineering; Pre-Medicine Curriculum, Dean's List Scholar*
Bachelor of Science candidate, May 2021

ENGINEERING EXPERIENCE

Research Assistant, The Pennsylvania State University Experimental Fluid Dynamics Lab for Rotating and Unsteady Systems

10/2020 – Present State College, PA

- Designing and constructing a compressed air wind tunnel for phase-locked wake imaging of flow on or near a rotor blade.
- Designing wide-angle diffuser screen conditions to prevent flow separation.
- Designing honeycombs and screens to minimize turbulence in flow conditioning.
- Converging nozzle design and geometry.

Stress Analysis Intern, Triumph Aerospace Structures – Vought Aircraft Division

05/2019 – 08/2019 Arlington, TX

- Developed "spring model" to analyze the distribution of stresses due to fasteners across the wing of the M100 Spacejet using VBA.
- Created a hardware database and updated a materials database for fasteners, screws, bolts, nuts, washers, etc. being used on the M100 Spacejet wing section.
- Updated buckling analysis and reverse engineered margins for pylon fittings.
- Assisted another intern in saving weight on a part using Patran.
- Trained in CATIA V5.

General Chemistry Tutor

08/2017 – 05/2019 Abington, PA

- Selected to tutor students on weekly lecture concepts.
- Prepared students for homework, quizzes and exams.

Organic Chemistry Undergraduate Teaching Assistant

08/2018 – 12/2018 Abington, PA

- Assisted organic chemistry students with classwork.

Evaluating and Testing of Mechanical Properties of 3D Printing Prosthetic Sockets

09/2017 – 05/2018 Abington, PA

- Explored recent developments in the use of 3D Printing technology to assist in the creation of transtibial prosthetic sockets.
- Received PSU ACURA **Honorable Mention** for outstanding achievement in undergraduate research.
- Poster presentation at the American Society of Biomedical Engineering and Biomechanics East Coast Conference, 2018.

SKILLS

- Analytical and critical thinking, structured problem-solving, productive in high-pressure environment, strategic planning.
- Software: SolidWorks, AutoCAD, Fusion360, MultiLab, CATIA V5, LabVIEW, Microsoft Word, PowerPoint, and Excel.
- Experience with C++, Matlab, Python – Pandas, NumPy, Matplotlib, Scikit-learn, Arduino, VBA, HTML, JavaScript - jQuery.

LEADERSHIP & INVOLVEMENT

- Personal project – QuestUni.com: online software platform that provides networking and research opportunities for university students.
- Secretary, American Institute of Aeronautics and Astronautics – Penn State Chapter.
- Member, Penn State Investment Association.
- Former Member, Penn State bowling and gymnastics club.
- 100+ hours volunteering with postoperative orthopedic surgery patients, supporting nursing staff, and shadowing various surgeries and medical procedures.

ACHIEVEMENTS & CERTIFICATES

- **Honorable Mention Award**: PSU Abington ACURA poster fair, and presented poster at the Biomedical Engineering and Biomechanics Conference at PSU Berks, Spring 2018.
- **Certificate of Achievement**: FAA Safety Team Aviation Learning Center Online Course: Part 107 Small Unmanned Aircraft Systems (Small UAS) Initial.

LANGUAGES

- Literacy in Hebrew.

INTERESTS

- Machine Learning
- Artificial Intelligence
- Rocket Propulsion
- Financial Markets
- Space Exploration
- Trading Automation
- Supersonics
- Drug Delivery
- Financial Modeling
- Piano